Optical Engineering 46(3), 035006 (March 2007)

Electronic equalizations for optical fiber dispersion compensation

Foster F. Dai
Auburn University
Electrical and Computer Engineering Department
200 Broun Hall
Auburn, Alabama 36849-5201
E-mail: fosterdai@auburn.edu

Abstract. This paper presents complete models for various fiber dispersions and their mitigations using electronic equalizers. A novel constant-modulus-adaptive (CMA) blind equalization technique is proposed for fiber dispersion compensation. Simulations demonstrated effective compensation means for chromatic and polarization mode dispersions using least-mean-square (LMS) and CMA blind equation techniques. Also proposed is the adaptive fiber transceiver architecture with eye-open-detect circuits that can be used to provide the feedback controls for adaptive thresholds and high-speed analog equalizers. [DOI: 10.1117/1.2715955]

Subject terms: fiber dispersion; chromatic dispersion; polarization mode dispersion; electronic equalization; constant-modulus-adaptive; blind equalization.

Paper 060399R received May 24, 2006; revised manuscript received Jul. 25, 2006; accepted for publication Aug. 22, 2006; published online Apr. 4, 2007.

1 Introduction

Since the early 1980s, the transmission speed of the optical networks has doubled almost every two years. When 10-Gigabits-per-second (Gb/s) optical networks were debated in the mid-1990s, many predicted that the 10-Gb/s-format would never become reality due to various obstacles. Similar debates now exist about the higher data rate at 40-Gb/s and the daring new concepts such as the agile optical network. The agile optical network is a reconfigurable optical network and is more resilient and more efficient compared to the traditional fixed point-point networks. However, in order to dynamically route an optical channel, an agile optical network requires dynamical dispersion management and adaptive dispersion compensation. One of the main concerns for high-data-rate agile optical networks is the dispersion effect in the optical fibers.

Modal, chromatic, and polarization mode dispersions are the major sources of transmission impairments in high-data-rate fiber communications. Without proper compensation, the performance of the fiber communication systems will be severely limited. The available dispersion compensation fiber is static in nature and therefore does not support agile optical networks. Other optical solutions are only capable of compensating one form of the dispersions with very high cost, high insertion loss, and slow tuning speed if they are tunable at all. The electronic equalizer can be dynamically tuned and has much smaller form factor and much lower cost.[1–4] An electronic equalizer can be integrated into a single chip using the high-speed *silicon germanium* (SiGe), *indium phosphorus*, or CMOS technologies. Further cost reduction is possible if the electronic equalizer and other receiver circuitry such as clock data recovery are integrated on the same die.

Blind channel identification and equalization approaches have received increasing attention in recent years because of their applications in wire line and wireless communications. Traditionally, a training sequence is transmitted during the acquisition mode to enable the receiver to program an equalizer or estimate the channel. For a time-varying dispersive channel, the training sequences may have to be transmitted periodically. The drawback of conventional equalizer algorithms lies on the fact that they all need the assistance of a training sequence. When the eye pattern of the channel output is initially closed, the conventional equalizer requires reference signals for channel estimation. On the other hand, blind equalization provides a reference-free equalization algorithm, which meets the current fiber communication transmission standard. Blind equalization is thus critical for agile optical networks with a time-varying channel environment.

Fiber dispersion includes both static *chromatic dispersion* (CD) and time-varying *polarization mode dispersion* (PMD) effects. In fiber networks with PMD, the channel dispersion characteristics constantly vary due to effects such as temperature variation and fiber stress and vibration. Traditional equalization methods using training patterns are thus not suitable for fiber polarization mode dispersion compensations. The impact of the modal dispersion and the first-order PMD on system performance in fiber networks is very similar to multipath interference in wireless systems, where blind equalization has been a common practice. Therefore, the blind equalization algorithm used in wireless systems can be applied to compensation of the modal dispersion and the first-order PMD. The second-order PMD is a combination of *depolarization* (DPLZ) and *polarization-dependent chromatic dispersion* (PCD). The second-order PMD is thus a wavelength-dependent dispersion, which does not have a similar countereffect in wireless communications. We will thus extend the prior art blind equalization techniques to include effects such as wavelength-dependent chromatic dispersion for high-data-rate fiber networks.

An electronic equalizer module is superior considering its cost, size, reliability, flexibility, and speed. A theoretical model of PMD compensation using digital signal processing was presented in Ref. 1 in which analog equalization

0091-3286/2007/$25.00

was not discussed. An integrated analog and digital signal processing technique implemented using both SiGe and CMOS technologies was presented in Ref. 2 for compensating dispersion in 10 Gb/s fiber networks. A seven-tap distributed transversal equalizer was implemented in a 0.18-μm SiGe BiCMOS process for 10-Gb/s multimode fiber optic links.[3] Both references were focused on integrated circuit designs without detailed equalization feedback algorithms. A hybrid opto-electronic equalizer optimized jointly using a least-mean-square algorithm was briefly presented in Ref. 4 The algorithm needs a training sequence and thus is not suitable for agile fiber networks. This paper presents adaptive electronic equalization means for the compensation of all forms of fiber dispersions, including modal, chromatic, and polarization mode dispersions. The proposed electronic equalizer employs a novel constant-modulus-adaptive-based blind equalization technique to achieve adaptive dispersion compensation without training sequence. Simulations demonstrate excellent dispersion compensations for various fiber dispersions such as CD and PMD. We will also discuss the adaptive fiber transceiver implementations for agile high-speed fiber networks.

The paper will start with a tutorial discussion on various fiber dispersions in Sec. 2. In Secs. 3, fiber channel emulation models with various dispersions will be developed. The proposed adaptive electronic equalization techniques with blind feedback algorithms are presented in Secs. 4 and 5. Finally, fiber dispersion compensations using the proposed electronic equalization approach will be demonstrated in simulation in Sec. 6.

2 Dispersion in Optical Fiber

Dispersion limits the bit-rate and transmission distance of fiber networks. Newly developed nonzero dispersion shifted fibers (*LEAF* and *TrueWave*) are mainly used in improving power and reducing fiber nonlinear effects. They fail to reduce dispersion in each separate channel, since dispersion is wavelength-dependent and accumulates at different rates. There are three main dispersion effects in optical fibers: (1) the modal dispersion; (2) the chromatic dispersion; and (3) the polarization mode dispersion.

2.1 *Modal Dispersion*

Modal dispersion occurs when light travels in multimode fibers that have core diameters of about 50 to 80 μm. In multimode fibers, each mode travels at a different speed for a given fiber length. The modal dispersion of a multimode fiber limits the signal transmission rate to about 100 Mbs/s over several kilometers. Due to the low cost and ease of connection, the multimode fiber is still the choice for short-reach optical connection. If cost is not a concern, single-mode fibers can be used to eliminate the modal dispersion.

2.2 *Chromatic Dispersion (CD)*

CD occurs in single-mode fibers due to the wavelength dependence of the light velocity. CD is inherent in fiber due to material refractive index and waveguide dispersion. Both the refractive index and group index vary with wavelength. Modern fiber exhibits both normal and anomalous dispersion regimes. For normal dispersion, blue wavelengths travel slower than red wavelengths. Anomalous dispersion reverses this order. An optical pulse is comprised of a range of wavelengths. CD impacts the pulse by retarding one color with respect to the other, causing pulse envelope spread.

Table 1 Maximum transmission distance limited by chromatic dispersion at $\lambda = 1550$ nm.

Fiber type	2.5 Gbs/s $\Delta\lambda = 0.025$ nm	10 Gbs/s $\Delta\lambda = 0.1$ nm	40 Gbs/s $\Delta\lambda = 0.4$ nm
SMF-28 $D \approx 17$ ps/nm/km	930 km	58 km	3.5 km
LEAF $D \approx 4$ ps/nm/km	4000 km	250 km	15 km

Data modulation of a single-wavelength laser causes the modulated laser spectrum to spread. An optical pulse in 10-Gbs/s format consists of a collection of photons with wavelength distribution spans over about 10 GHz and will travel along the fiber at different speeds. After some distance, the difference in speed will cause noticeable pulse spread in time and result in possible wrong detection at an optical receiver. Assuming electrical field of a linearly polarized light wave in a single mode-fiber is given by $E = E_0 e^{i[\beta(\omega)z - \omega t]}$, where $\beta(\omega) = n(\omega)\omega/c$ is the propagation constant at angular frequency ω and the group velocity v_g is defined as $v_g^{-1} = \beta_1 = d\beta/d\omega$. The frequency-dependent group velocity, i.e., the *group velocity dispersion* (GVD), leads to pulse broadening of

$$\Delta T = \frac{dT}{d\omega}\Delta\omega = \frac{d}{d\omega}\left(\frac{L}{v_g}\right)\Delta\omega = L\frac{d^2\beta}{d\omega^2}\Delta\omega = LD\Delta\lambda \tag{1}$$

where $D = dv_g^{-1}/d\lambda = -(2\pi c/\lambda^2)(d^2\beta/d\omega^2)$ is defined as the *dispersion parameter* in units of ps/km/nm. In the absence of non-linearity, pulse propagation and dispersion can be described with the first few terms of the Taylor series of $\beta(\omega)$ at the interested frequency ω_0 as

$$\beta(\omega) \approx \beta_0 + \beta_1(\omega - \omega_0) + \beta_2(\omega - \omega_0)^2/2 + \beta_3(\omega - \omega_0)^3/6 \tag{2}$$

where ω_0/β_0 is the phase velocity, $1/\beta_1$ is the group velocity, $\beta_2 = d^2\beta/d\omega^2$ is the GVD parameter, and $\beta_3 = d^3\beta/d\omega^3$ is related to the dispersion slope. CD is caused by the variation in the group velocity with respect to the frequency. β_2 and β_3, in practice, describe the measurable CD in an optical fiber.

CD limits the maximum distance of a signal transmitted without regeneration. The estimated chromatic dispersion limit of a signal with data rate of B and bandwidth of $\Delta\lambda$ is given by $L_D = 1/(BD\Delta\lambda)$. The CD limited maximum transmission distance at $\lambda = 1550$ nm for two most popular optical fibers from Corning are listed in Table 1.

To overcome CD, *dispersion compensation fiber* (DCF) is normally used. DCF can introduce signal power loss. For example, to compensate the CD of 50 km of SMF-28 fiber (the standard single mode fiber), the compensation module

consists of 15 km of DCF and introduces about 7-dB insertion loss. To recover that loss, extra-expensive optical amplifiers have to be used. DCF is static in nature. It cannot compensate the dynamically changing dispersion associated with re-configurable fiber networks. Moreover, DCF can only compensate one type of dispersion, namely, the chromatic dispersion.

A few tunable optical means such as free-space resonant cavity device[5] and *fiber Bragg grating* (FBG)-based devices[6] have been reported for CD compensation. The free-space resonant cavity device has insertion loss larger than 10 dB, and the tuning is performed via mechanical method that potentially can be a reliability concern. All of the FBG-based devices are channel-dependent. For a DWDM system, there could be up to 200 optical channels assigned to a single fiber; it is clearly a logistic problem to manage that many different FBG components, not to mention the high cost required by FBG devices on a per-wavelength basis. The FBG-based compensators do not allow the dynamic allocation of optical channels and hence they do not support re-configurable λ-switched networks. Although it is possible to produce optical fiber with near-zero CD, the large loss associated with zero dispersion fiber makes it almost useless in long-haul fiber networks. On the other hand, a DWDM system actually demands a certain amount of CD to minimize the fiber nonlinear effects such as the stimulated Brillouin scattering.

2.3 *Polarization Mode Dispersion*

An ideal optical fiber has a circular cross section such that an optical field propagating in a fiber would experience the same propagation characteristics regardless of the orientation of the incoming optical field. Unfortunately, real fibers are noncircular and take on a slightly elliptical shape due to either imperfect manufacturing process or unavoidable nonsymmetrical stress in deployed environment. Even worse, the elliptical shape varies along the fiber and is also affected by the environmental temperature and vibration. Such a condition produces two different polarization modes with different phase/group velocities even in a single-mode fiber. The accumulated result to the first order is a relative time delay for two orthogonal polarizations at the fiber output.

PMD is caused by an optical fiber's randomly varying birefringence. To the first order, PMD can be represented by a *differential group delay* (DGD) between two principal states of polarization (PSP) of the optical fiber. Group velocity dispersion due to PMD can be expressed as

$$\Delta T = |L/v_{g1} - L/v_{g2}| = L|\beta_1' - \beta_2'| = L\Delta\beta' \tag{3}$$

where $\Delta\beta(\omega)=\Delta n(\omega)\omega/c$ comes from the fiber birefringence. Due to the random nature of manufacturing process and the stress field, polarization mode dispersion in a long fiber has a square root of length dependence. Polarization mode dispersion is proportional to $D_{\mathrm{PMD}}\sqrt{L}$, where L is the length of the fiber, and D_{PMD} is the dispersion parameter for the fiber in unit ps/$\sqrt{\mathrm{km}}$. Unlike the chromatic dispersion, the PMD dispersion parameter is dependent upon not only the quality of fiber but also the installation environment and may vary when ambient temperature changes or vibration occurs. With the improvement of fiber manufacturing, fiber PMD has been greatly reduced in recent deployed fibers. Corning SMF-28 standard single-mode fiber made in 2001 has a maximum PMD of 0.2 ps/$\sqrt{\mathrm{km}}$ for individual fibers. However, about 30% of the total fiber networks were deployed before 1993, which has high PMD of 1 ps/$\sqrt{\mathrm{km}}$. In Table 2, the maximum optical transmission distance (km) limited by PMD is listed, where the EDFA and CDC dispersion parameter is assumed to be 0.141 ps/$\sqrt{\mathrm{km}}$ and the maximum tolerable PMD without PMD compensation (PMDC) is assumed to be 15% of the data period. According to Table 2, at 10 Gb/s, the transmission distance is severely limited by PMD for old fibers laid out before 1993. At 40 Gb/s, the transmission distance is severely limited by PMD for any fibers manufactured based on today's technology. PMD compensation devices are still at the early research and development stage, with most teams working on various expensive optical solutions.

Table 2 Maximum transmission distance limited by polarization mode dispersion.

Fiber Type/Data Rate	2.5 Gbs/s	10 Gbs/s	40 Gbs/s
Bad fiber (made before 1993) $D_{\mathrm{PMD}}\approx 1$ ps/$\sqrt{\mathrm{km}}$	2763 km	173 km	11 km
Good fiber (made after 1993) $D_{\mathrm{PMD}}\approx 0.5$ ps/$\sqrt{\mathrm{km}}$	8750 km	547 km	34 km
Best fiber (made after 2000) $D_{\mathrm{PMD}}\approx 0.25$ ps/$\sqrt{\mathrm{km}}$	23,497 km	1469 km	92 km

As illustrated in Fig. 1, PMD can be represented as a vector $\vec{\tau}=\tau\cdot\hat{p}$, where the magnitude of the PMD vector stands for DGD, which is the time delay between orthogonal pulses. The direction of the PMD vector is represented by the unit Stokes vector $\hat{p}$ in the direction of PSP. The PMD vector cannot, in general, be represented on the *Poincaré* sphere, as its length is other than unity. As the PSPs change the pointing direction with frequency, so does the PMD vector. Also, as the frequency changes, the vector length can change as well. Expanding the PMD vector around the interested frequency ω_0, we have

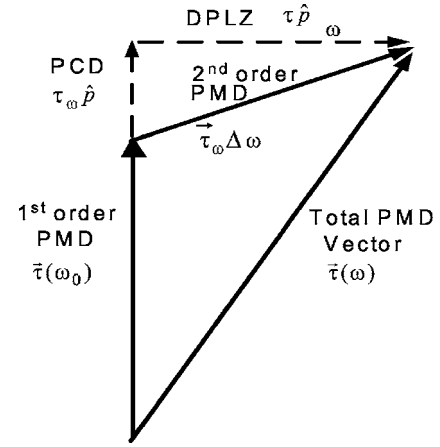

Fig. 1 Vector representation of first-order and second-order PMD.

$$\vec{\tau}(\omega) = \vec{\tau}(\omega_0) + \{\tau_\omega \hat{p} + \tau \hat{p}_\omega\}(\omega_0 - \omega) + \ldots , \quad (4)$$

where $\vec{\tau}_{\omega_i} = \tau_\omega \cdot \hat{p}$ represents polarization-dependent chromatic dispersion (PCD) and $\tau \hat{p}_\omega$ denotes the frequency-dependent PSP, namely, depolarization (DPLZ) components since the direction of DPLZ is perpendicular to the original PSP. The combined first-order and second-order PMD vector representation is given in Fig. 1. Mean DGD of the first-order PMD increases as square root of length. However, the mean of second-order PMD (SOPMD) is proportional to length. In case of high DGD, second-order impairment is relatively higher. SOPMD effect is enhanced in case of prechirped sources or high residual chromatic dispersion. Among the second-order component, PSP change with respect to frequency (depolarization) is dominant.

Recall that DGD is the length of the PMD vector and indicates the temporal delay between "fast" and "slow" input pulses. A large ensemble of fibers exhibiting birefringence will show a range of DGD values for a particular optical frequency. The histogram of those DGD values follows a Maxwellian distribution.[7,8] The original of Maxwellian distribution is where there are three Gaussian distributions along three orthogonal coordinates. The PMD vector is projected onto the three coordinates. The origin of Gaussian distributions comes from the "random walk" the PMD vector takes over the length of a long PMD fiber. For a fixed PMD, DGD is a random variable that has a Maxwellian *probability density function* (PDF) as follows:

$$pdf_{\mathrm{PMD1}}(x) = \left(\frac{8}{\pi^2 \tau}\right)\left(\frac{2x}{\tau}\right)^2 \exp\left[-\frac{(2x/\tau)^2}{\pi}\right]. \quad (5)$$

The statistics of magnitude *second-order PMD* (SOPMD) are derived in a similar manner to DGD statistics. The component PDFs for SOPMD follows the soliton amplitude, a "sech" function.[8] The magnitude SOPMD is the magnitude of the three components and is presented as a scalar. The PDF of the SOPMD can be expressed as a "sech tanh" form as

$$pdf_{\mathrm{PMD2}}(x) = \left(\frac{8}{\pi \tau^2}\right)\left(\frac{4x}{\tau^2}\right)\tanh\left(\frac{4x}{\tau^2}\right)\mathrm{sech}\left(\frac{4x}{\tau^2}\right). \quad (6)$$

Associated with SOPMD are the component vectors. That is, the SOPMD vector can be resolved onto the original PMD vector. The parallel component is the change of DGD with frequency, namely, the PCD. The perpendicular component is the change of PSP direction with frequency scaled by the local DGD, namely, the depolarization. Depolarization is the more deleterious effect of SOPMD. When the pointing direction of the PMD changes with frequency, it is difficult to anti-align an optical PMD compensator to the PMD vector. There is no analytic expression for the depolarization PDF.[9] However, the PDF of polarization-dependent chromatic dispersion can be expressed as

$$pdf_{\mathrm{PCD}}(x) = \left(\frac{4}{\pi \tau^2}\right)\mathrm{sech}^2\left(\frac{4x}{\tau^2}\right), \quad (7)$$

which is shaped like the soliton amplitude.[8] The statistics of various fiber dispersions can be considered in the blind equalization algorithm.

3 Fiber Dispersive Channel Models

In order to establish a simulation environment for dispersion compensation analysis, we need to truthfully emulate fiber channel dispersive performance.

3.1 *Emulation of Chromatic Dispersion*

CD is caused by the wavelength dependence of the light propagation constant. For Corning SMF-28 standard single-mode fibers, the wavelength dependence of the dispersion parameter D in unit [ps/(nm*km)] is given as

$$D = \frac{S_0(\lambda - \lambda_{\mathrm{ZD}}^4/\lambda^3)}{4}, \quad (8)$$

where λ_{ZD} is the zero dispersion wavelength and S_0 is the dispersion slope at the zero dispersion wavelength λ_{ZD}. The dispersion slope for SMF-28 fiber can be determined as

$$S = \frac{dD}{d\lambda} = \frac{S_0(1 + 3\lambda_{\mathrm{ZD}}^4/\lambda^4)}{4}. \quad (9)$$

The second order and third order propagation constants are given as follows:

$$\beta_2 = \frac{-D}{(2\pi c/\lambda^2)}, \quad \beta_3 = \frac{S - 4\pi c \beta_2/\lambda^3}{(2\pi c/\lambda^2)^2}. \quad (10)$$

qNeglecting wavelength-independent β_1, the light propagation distorted by chromatic dispersion can be modeled as

$$A(z,t) = \frac{1}{2\pi}\int_{-\infty}^{\infty} \tilde{A}(0,\omega)\exp\left[\frac{i}{2}\beta_2 z\omega^2 + \frac{i}{6}\beta_3 z\omega^3 - i\omega t\right] d\omega, \quad (11)$$

where $\tilde{A}(0,\Delta\omega)$ is the spectrum of the undistorted input signal $A(0,t)$.

In the CD emulator for SMF28 single-mode fibers, the zero dispersion wavelength $\lambda_0 = 1312$ nm; typical dispersion slope at $\lambda_{\mathrm{ZD}} S_0$ is 0.092 [ps/(nm^2*km)]. Figure 2 shows the eye diagrams distorted by chromatic dispersions for SMF-28 fiber with fiber lengths of 75 km and 100 km, respectively. Light wavelength $\lambda = 1550$ nm. We can see that the longer the fiber is, the more severe the dispersion is. For a fiber length of 100 km, the eye opening magnitude is only about 0.25, assuming the undistorted eye opening is 1.

3.2 *Emulation of the First-Order PMD*

The first-order PMD is wavelength-independent and is caused by different propagation speed along principal polarization directions. Emulation of the first-order PMD can be modeled in Matlab Simulink as shown in Fig. 3. The input signal is split into two principal polarization states with a relative power splitting ratio of gamma (γ). The signal with amplitude $\sqrt{\gamma}$ is delayed by DGD seconds, while another signal with amplitude $\sqrt{1-\gamma}$ has zero delay. Both signals are then recombined based on vector addition. Output {Out1} is the intensity of the recombined signal. By randomizing γ, the effect of polarization scrambling can

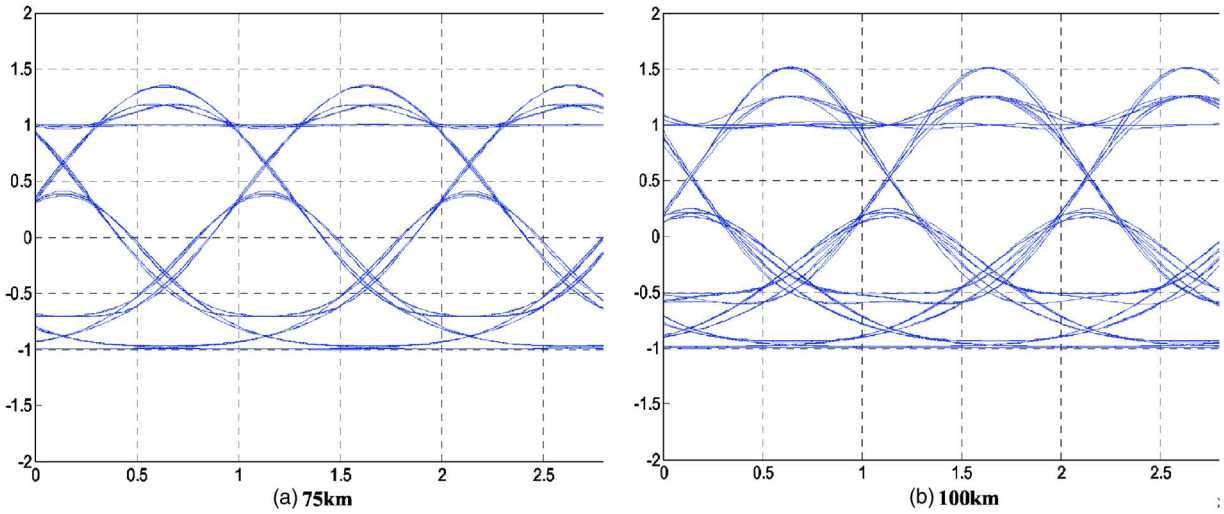

Fig. 2 Eye diagrams distorted by chromatic dispersions for SMF-28 fiber.

also be emulated. To emulate the first-order PMD, we choose the relative power ratio $\gamma=50\%$, which represents the worst-case PMD.

Figure 4 shows the simulated eye diagrams of the 40-Gb/s random signal after the first-order PMD emulator with (1) DGD=15 ps, and (2) DGD=25 ps, which equals the period of 40-Gb/s date. A fourth-order Bessel low-pass filter with cutoff frequency at data rate (40 GHz) is used after the emulator. For different DGD values, the simulated distorted eye diagrams are compared with the measured eye patterns generated under the same PMD conditions (40 Gb/z NRZ 231-1 PRBS). The simulated PMD distorted eye patterns agree with the measured eyes quite well. Note that no Gaussian noise has been added in the simulation. Thus, the simulated eye patterns appear as smooth curves. Gaussian ASE noise can also be added based on the different noise variances for ON and OFF signals.

3.3 *Emulation of the Second-Order PMD*

As discussed, the second-order PMD is wavelength-dependent. It has first-order PMD components and is affected by CD as well. To model the distributed random effect of the PMD, Monte Carlo simulations using a fiber waveplate model are used to generate the PMD impaired fiber. A waveplate is a birefringent medium that propagates various incoming polarizations with various time delays. The maximum and minimum time delays are expressed by the eigenstates of the waveplate. The emulator consists of N number of waveplates that have a fixed DGD $\Delta\tau_p$. The model can also be extended to include a birefringent section with varying DGD. The optical axes of the waveplates are rotated randomly relative to each other, as shown in Fig. 5. The resultant PMD emulator has an average DGD of $\Delta\tau=\sqrt{8N/3\pi}\Delta\tau_p$, with the appropriate first- and second-order PMD statistics.[8]

The concatenated birefringent waveplates can be mathematically expressed by a complex two-dimensional unitary matrix, known as the Jones matrix. The input and output optical signals can also be expressed using Jones complex vectors. The unitary propagation matrix and the complex vectors are dependent on wavelength and can thus model the second-order PMD. In addition, other fiber impairments such as loss, linear dispersion, and nonlinearities can also be added into the model. The second-order PMD is modeled in the frequency domain. The resulting field components are then transformed back to the time domain. Signal propagation is accomplished by multiplying the resulting Jones matrix for the concatenated birefringent sections and operating on an incoming input optical field at each frequency, as expressed by

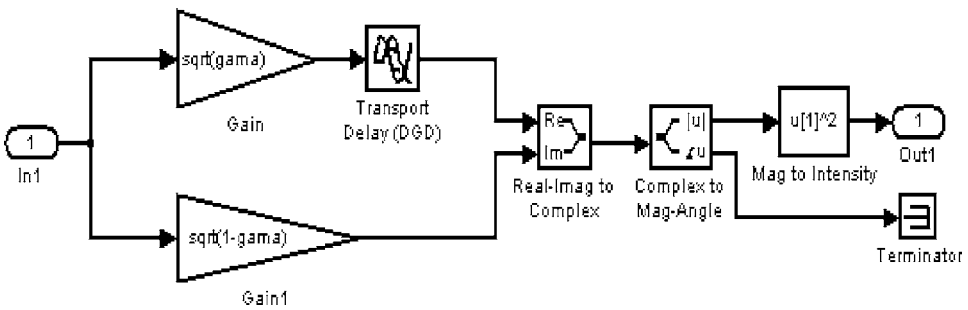

Fig. 3 The first-order PMD emulator with power splitting ratio (gamma) and differential group delay (DGD) as input parameters.

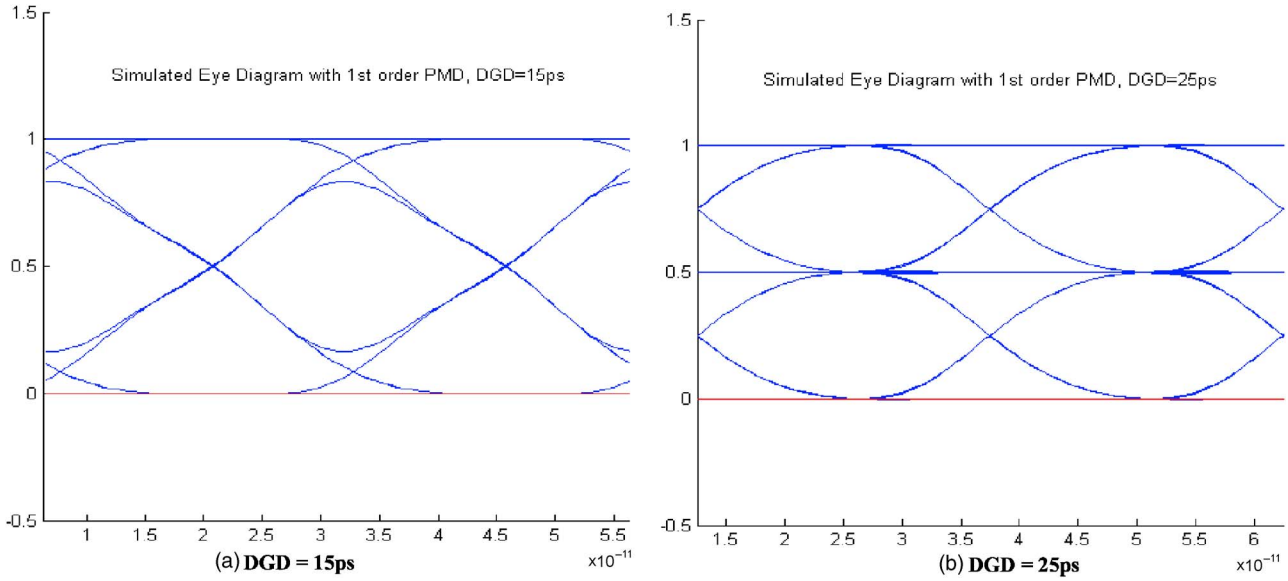

Fig. 4 Simulated eye diagrams of 40-Gb/s random signal after first-order PMD emulator with (a) γ =0.5 and DGD=15 ps, (b) γ=0.5 and DGD=25 ps.

$$\begin{bmatrix} E_x^o(\omega_k) \\ E_y^o(\omega_k) \end{bmatrix} = \begin{bmatrix} u_1(\omega_k) & u_2(\omega_k) \\ -u_2^*(\omega_k) & u_1^*(\omega_k) \end{bmatrix} \begin{bmatrix} E_x^i(\omega_k) \\ E_y^i(\omega_k) \end{bmatrix}, \tag{12}$$

where u^* represents the complex conjugate of the matrix element u. The total propagation matrix at frequency ω_k is obtained by multiplying the Jones matrixes of individual waveplates as

$$\begin{bmatrix} u_1(\omega_k) & u_2(\omega_k) \\ -u_2^*(\omega_k) & u_1^*(\omega_k) \end{bmatrix} = \prod_{i=1}^{N} R_i^T D_i R_i = \prod_{i=1}^{N} \begin{bmatrix} \cos(\theta_i) & -\sin(\theta_i) \\ \sin(\theta_i) & \cos(\theta_i) \end{bmatrix} \times \begin{bmatrix} e^{j\phi_i(\omega_k)/2} & 0 \\ 0 & e^{-j\phi_i(\omega_k)/2} \end{bmatrix} \times \begin{bmatrix} \cos(\theta_i) & \sin(\theta_i) \\ -\sin(\theta_i) & \cos(\theta_i) \end{bmatrix}, \tag{13}$$

where index $i=1,2,\ldots,N$ represents different waveplate; $\phi(\omega_k)=\tau\omega_k$ for $k=1,2,\ldots,M$ frequencies; τ is the DGD; and θ_i is the rotation angle of the ith waveplate.

PMD parameters such as differential group delay (DGD), polarization-dependent chromatic dispersion (PCD) are related to the Jones matrix components as follows:[10,11]

$$\mathrm{DGD} = 2\sqrt{|u_1'(\omega)|^2 + |u_2'(\omega)|^2}, \quad \text{or}$$

$$\mathrm{DGD} = |\mathrm{Arg}(\rho_1/\rho_2) \big/ \omega_{i+1} - \omega_i|,$$

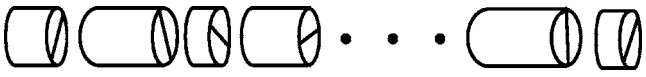

Fig. 5 Waveplate model for emulation of fiber PMD.

$$\mathrm{PCD} \approx \frac{\mathrm{DGD}(\omega_{i+1}) - \mathrm{DGD}(\omega_i)}{\omega_{i+1} - \omega_i}, \tag{14}$$

where ρ_1 and ρ_2 are the eigenvalues of the matrix product $T(\omega_{i+1}) \cdot T^{-1}(\omega_i)$. The last equation represents the derivative of DGD with respect to frequency. The total second-order PMD vector magnitude (SOPMD) is determined by first finding the output PMD vector $\vec{\tau}$ as a function of frequency for the resultant system expressed by the Jones matrix and

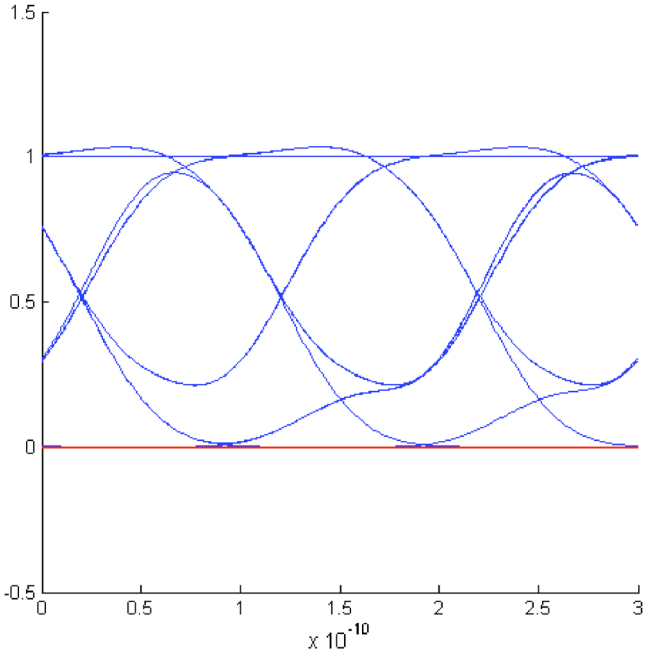

Fig. 6 Eye diagrams distorted by second-order PMD with DGD =70.568 ps, PCD=304.16 ps^2, DPLZ=2004.15 ps^2, SOPMD =2027.1 ps^2.

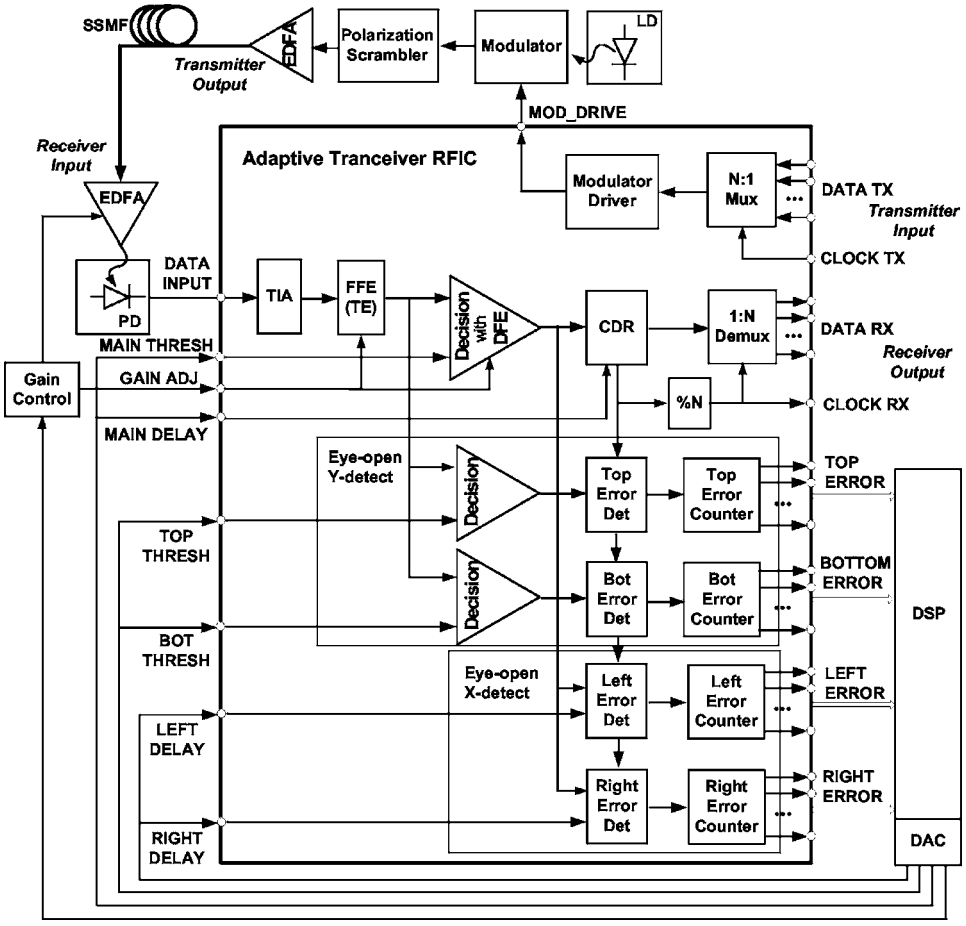

Fig. 7 Schematic diagram of an integrated adaptive fiber transceiver with analog equalizers for fiber dispersion compensation.

then its variation rate, i.e., the derivative with respect to frequency can be found by

$$\mathrm{SOPMD} \approx \frac{\vec{\tau}_{i+1} - \vec{\tau}_i}{\omega_{i+1} - \omega_i}. \tag{15}$$

Note that the two orthogonal components of the total SOPMD vector are the PCD and the depolarization (DPLZ). The depolarization can thus be obtained by

$$\mathrm{DPLZ} = \sqrt{|\mathrm{SOPMD}|^2 - |\mathrm{PCD}|^2}. \tag{16}$$

Figure 6 gives a simulated eye diagram distorted by second-order PMD with DGD=70.568 ps, PCD= -304.16 ps^2, DPLZ=2004.15 ps^2, and SOPMD =2027.1 ps^2. In the simulation, 10,000 fibers are used to emulate the random statistics of fiber PMD. Each fiber section consists of 12 waveplates with 10-ps delay to model the distributed dispersion effect of the fiber.

4 Adaptive Electronic Equalizations

As shown, fiber communication is limited by transmission impairments due to fiber dispersions. Optical devices are only capable of compensating one form of the dispersions with very high cost, high insertion loss, and slow tuning speed if they are tunable at all. In contrast, electronic equalizers are low cost, tunable, and capable of compensating all forms of fiber dispersions. Figure 7 shows an integrated adaptive fiber transceiver with analog equalizers for fiber dispersion compensation.[12] During operation, data transmitted at lower rates can be fed in a parallel fashion into an N:1 multiplexer, which generates a relatively high-transmission-rate data stream. The data stream can then be amplified by a modulator driver for driving external optical modulator. Polarization scrambler can be inserted after optical modulator to randomize the polarization direction of the transmitted light. When light intensities along the principal polarization directions are the same, the system suffers a maximum power penalty due to PMD. Thus, by scrambling the polarization of the transmitted optical signal, the average PMD related power penalty is reduced because of a lower probability that the system will be locked in states with large power penalties. *Erbium doped fiber amplifier* (EDFA) can be inserted after the scrambler to provide sufficient power for transmission of the optical signal along a *standard single-mode fiber* (SSMF).

On the receiver side of the circuit, another EDFA is used to compensate for gain lost during transmission and also provides an overall gain control so that *photo-detector* (PD) and front-end amplifier can operate in their proper dynamic ranges. The received optical signal is converted to electrical signal using a PD. A *trans-impedance amplifier* (TIA) is

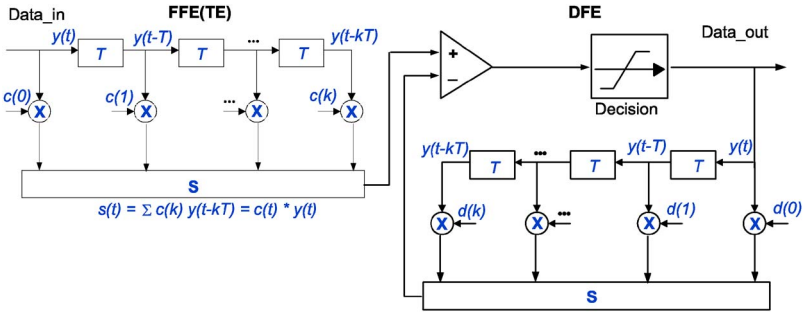

Fig. 8 An analog electronic equalizer including TE and DFE.

used to convert the electrical current mode signal to voltage mode signal. After the decision stage, the data stream can be used to recover the clock, which is synchronized with the data. Clock and data recovery circuitry can be embedded in an adaptive receiver. The receiver IC preferably detects errors occurring during data detection and adjusts the decision thresholds adaptively. Error detection can include top and bottom error detectors, and respective top and bottom error counters. Error detection can also include left and right error detectors, and respective left and right error counters. The detected error signals indicate the degree of eye opening and are processed by a digital signal processing chip embedded with the equalization algorithms. A DAC provides the analog feedback control signals needed for adaptive thresholds and equalizer tap coefficients.

The high-speed analog electronic equalizers can be implemented in SiGe and CMOS technologies.[2,12] Figure 8 further illustrates analog electronic equalizers including a *feed forward equalizer* (FFE) and *decision feedback equalizer* (DFE). The voltage signal output from the TIA is fed to the data input of the FFE, which performs the dispersion compensation for the distorted voltage signal. The output of the FFE is experienced additional compensation at the DFE. The compensated signal is then fed into a clock data recovery block to recover the data clock. FFE, a linear equalizer, is used to compensate for moderate amplitude distortion. On the other hand, a decision feedback equalizer is used to improve receiver performance in the presence of moderate to severe amplitude distortion. A DFE is intrinsically nonlinear as it feeds back to the input a sequence of hard decisions made at the equalizer output. The feedback section removes the lagging intersymbol interference that is beyond the reach of the forward section. However, the DFE suffers from the problem of error propagation since hard decisions may destroy information: once a wrong decision is made, errors are fed back to the equalizer input, which in turn leads to a higher probability of error on subsequent decisions. The end result is a burst of errors. Moreover, like any feedback system, a DFE design involves stability analysis, while an FFE is always stable.

The performance of an analog electronic equalizer is limited by the circuit linearity and bandwidth. The equalizer circuit should have minimum group delay in order to minimize the additional dispersion due to the equalizer. The implementation of the high-speed equalizer is not easy even at 10 Gb/s, and it is very challenging at 40 Gb/s.[13] Even if the equalizer itself can be implemented for high-data-rate applications, the feedback circuits cannot operate at the data rate, since complicated calculations need to be done within one clock cycle. Fortunately, fiber dispersion is either a time-invariant (e.g., CD) or slow time-variant (e.g., PMD) process. The feedback circuit thus needs only operate at a much slower frequency than the data rate. The input to the feedback block can be an accumulated averaged data, as illustrated in Fig. 7. The tap coefficients of the equalizer are thus updated at a much slower frequency as well. An alternate approach is to sample the input distorted signal using a high-speed *analog-to-digital converter* (ADC), if such as a converter is available. Thus, all the equalizations, and error corrections plus equalization feedback algorithms can be implemented digitally, providing a more accurate and higher performance alternative to analog equalizers. The digital equalization approach is illustrated in Fig. 9.

5 Feedback Algorithm for Electronic Equalizers

Various adaptive equalizer algorithms have been developed for digital signal processing. LMS maximum likelihood algorithms are widely used in equalizer designs. *Recursive least-squares* (RLS) algorithm achieves faster convergence, but is computationally more complex than LMS since matrix inversion is required. The reference signal required by the LMS algorithm can be either provided by a transmitted training sequence or estimated by the detected bits. Decision-directed tap adaptation uses the output of the slicer/decision circuit as an estimation of the transmitted sequence. LMS is simple and can be implemented for FFE and DFE equalizations.[17–19] For higher data rates, the steepest descent algorithm can be used, which consecutively dithers the equalizer taps to achieve the optimized signal quality. As a simplified variant of LMS, sign-sign LMS

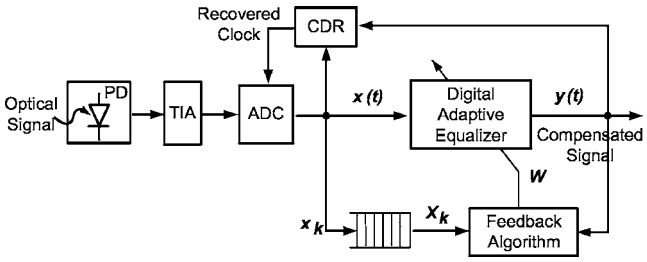

Fig. 9 A digital electronic equalizer with assistance of a high-speed ADC.

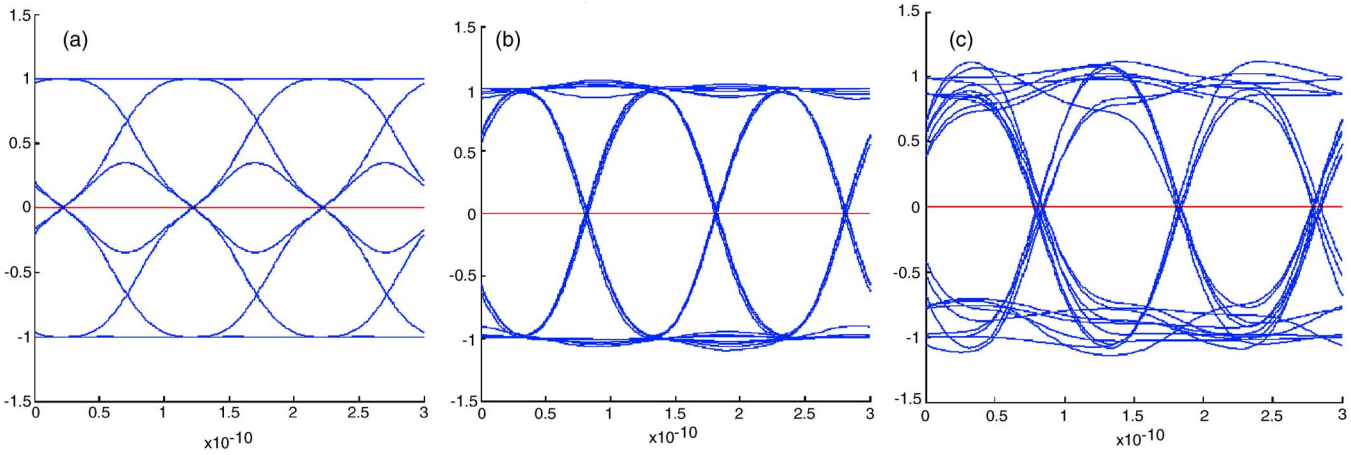

Fig. 10 PMD compensation using a 7-tap analog FFE. (a) Eye diagram distorted by first-order PMD with power splitting ratio=0.5 and DGD=0.8 period. (b) Compensated eye diagram with LMS adaptive feedback. (c) Compensated eye diagram with fixed tap coefficients.

algorithm evaluates only the signal signs, which has greatly reduced computation time, yet with very "noisy" gradient estimate. The biggest advantages of sign-sign LMS algorithm is that it does not require any high-speed ADC and thus can be implemented at high speed.

The drawback of conventional equalization algorithms lies on the fact that they need the assistance of a training sequence, which is not suitable for applications with a varying channel environment. On the other hand, blind equalization provides a reference-free equalization algorithm, which meets the current fiber communication transmission standard. Blind equalization is thus critical for agile optical networks, where the channel environment varies constantly. Since binary ON-OFF key modulation with constant envelope is used in fiber communication system, *constant-modulus adaptive algorithm* (CMA) is proposed for fiber dispersion compensation using blind equalization.[14] The key to the success of a blind equalization is the efficient error estimation through built-in eye-open detection circuits such as the one proposed in the previous section.

5.1 *LMS Equalization*

If a reference training sequence is transmitted during a preassigned time slot, the equalizer coefficients can be adapted by using the LMS adaptive algorithm so that the output of the equalizer closely matches the training sequence. The LMS reference can also be estimated by the detected bits. In this case, a blind equalization is implemented with the goal of widening the eye-open for improved BER. If r_k is the reference signal and y_k is the equalizer output at time instance k, respectively, the error signal of LMS is defined as

$$e_k = r_k - y_k = r_k - W_k^T X_k, \tag{17}$$

where X_k is the equalizer input signal and W_k is the equalizer tap coefficients at time instance k, respectively. The cost function to be minimized is defined as

$$J_k = e_k^2 = (r_k - W_k^T X_k)^2. \tag{18}$$

In each iteration, the gradient is estimated by

$$\nabla J_k = \frac{\partial J_k}{\partial W_k} = 2e_k \frac{\partial e_k}{\partial W_k} = -2e_k X_k. \tag{19}$$

With the steepest descent adaptive algorithm and a bounded step size μ, the equalizer tap coefficients can thus be adapted as follows:

Table 3 TAP coefficients of 3-, 5-, and 7-tap LMS FFE for first-order PMD compensation with DGD=0.25%, 0.5%, and 0.75% symbol period.

DGD	25%	50%	75%
C1 of 3-tap FFE	0.001295	−0.03202	−0.3023
C2 of 3-tap FFE	1.185	1.2	1.515
C3 of 3-tap FFE	−0.2147	−0.1914	−0.2791
C1 of 5-tap FFE	0.00003686	0.001223	0.06619
C2 of 5-tap FFE	0.0009815	−0.03445	−0.3336
C3 of 5-tap FFE	1.187	1.204	1.532
C4 of 5-tap FFE	−0.2232	−0.197	−0.3061
C5 of 5-tap FFE	0.04044	0.03116	0.05649
C1 of 7-tap FFE	0.0001306	−0.0002302	−0.0153
C2 of 7-tap FFE	0.0001521	0.001364	0.07292
C3 of 7-tap FFE	0.0009156	−0.03417	−0.3367
C4 of 7-tap FFE	1.187	1.204	1.543
C5 of 7-tap FFE	−0.2236	−0.1972	−0.3088
C6 of 7-tap FFE	0.042	0.03221	0.06169
C7 of 7-tap FFE	−0.007656	−0.005136	−0.01132

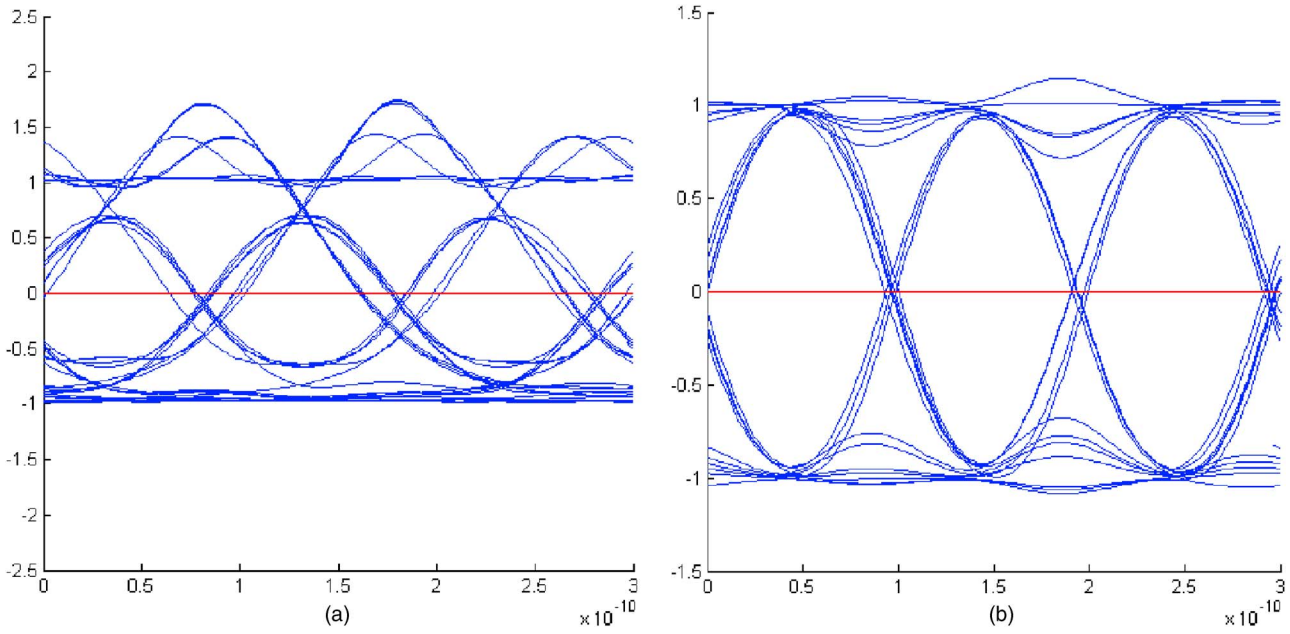

Fig. 11 CD compensation using a 7-tap analog FFE. (a) Eye diagram distorted by CD after transmission in a 75-km SMF-28 fiber at wavelength 1550 nm. (b) Compensated eye diagram with LMS adaptive feedback.

$$W_{k+1} = W_k - \mu \nabla J_k = W_k + 2\mu e_k X_k. \tag{20}$$

5.2 *CMA Blind Equalization*

Inclusion of the training sequence with the transmitted information adds an overhead and thus reduces the throughput of the system. Therefore, to reduce the system overhead, adaptation schemes are preferred that do not require training, i.e., blind adaptation schemes.[15] In blind equalization, instead of using the training sequence, one or more properties of the transmitted signal are used to estimate the inverse of the dispersive channel. Unlike the LMS algorithm, which assumes a reference r_k, the error e_k in Eq. (17) cannot be used to define the cost function in blind equalization. Since the transmitted signal in fiber communication is of the constant amplitude, we can assume constant amplitude A in the absence of signal degradations. Then, the error signal in blind equalization can be defined as

$$e_k = |y_k|^2 - A^2. \tag{21}$$

The cost function can be further defined as[16]

$$J_k = \mathrm{E}\{e_k^2\} = \mathrm{E}\{(y_k^2 - A^2)^2\}. \tag{22}$$

The true gradient of J at time step k can be approximated by its instantaneous value as

$$\nabla J_k = \frac{\partial J_k}{\partial W_k} = 2e_k \frac{\partial e_k}{\partial W_k} = 4e_k y_k X_k = 4(y_k^2 - A^2) y_k X_k. \tag{23}$$

The CMA recursion expression becomes

$$W_{k+1} = W_k - \mu \nabla J_k = W_k - \mu(y_k^2 - A^2) y_k X_k, \tag{24}$$

where the equalizer output is $y_k = W_k^T X_k$.

6 Simulation Results

6.1 *LMS Equalizer*

To demonstrate the effect of an electronic equalizer on fiber dispersion compensation, we simulated a 7-tap analog feed forward equalizer (FFE) with LMS feedback algorithm for PMD compensation (Fig. 10) and chromatic dispersion compensation (Fig. 11). Note that the severely distorted signal can be compensated using just 7 taps in an analog transversal equalizer. With the adaptive feedback, the tap coefficients are constantly adjusted based on the error signal. Even without feedback, the fixed coefficient equalizer can still open the distorted eye. For a fixed network, we can thus predetermine the equalizer tap coefficients and load them into the equalizer at the field, which is very attractive from a cost reduction point of view. For chromatic dispersion, tap coefficients can be programmed based on the length and type of the fiber, providing a much more economic way than the current solution using dispersion compensation fiber (DCF), which is static and also wavelength-dependent. As a reference for practical designs, we summarize in Table 3 the tap coefficients of 3-, 5-, and 7-tap LMS transversal equalizers for first-order PMD compensation with DGD=0.25%, 0.5%, and 0.75% of the symbol period, respectively.

6.2 *CMA Blind Equalizer*

In simulation for blind equalization, we set signal amplitude A to 1 and normalized the input signal to the range of $[-1, 1]$. Baud-Spaced CMA (sampling period equal to the symbol period) is used, and tap coefficient W_0 is initialized to be "Single-Spike"[15] (one nonzero tap coefficient, and all other to 0). Three scenarios with different settings of DGD are investigated. Symbol period is set to be 0.025 nsec (25e−12 seconds). Simulation results for DGD of 80% of

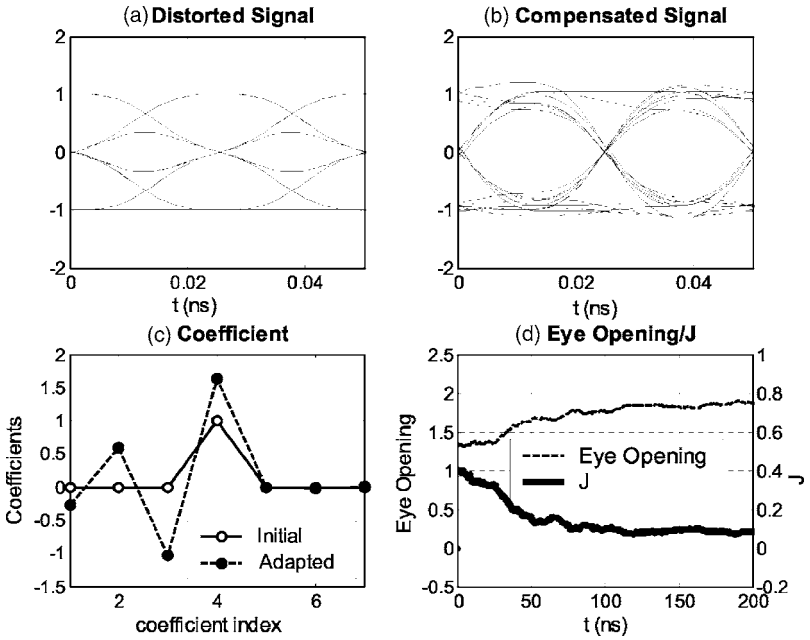

Fig. 12 CMA blind equalization for first-order PMD compensation with DGD=80% symbol period.

the symbol period are shown in Fig. 12. In all scenarios, feedback gain μ is set to 0.005. In Fig. 12(a) and 12(b), show the eye diagrams before and after the compensation; (c) gives the initial and adapted tap coefficients; and (d) plots the eye opening and the cost function J, which is defined in (22) and ideally converges to 0. Assuming the eye is constant along the horizontal direction, the eye-open is then measured as the vertical height between the mean of peak amplitudes and the mean of valley amplitudes, which converges to value 2 ideally. Note that when DGD is 80% of the symbol period, it takes more than 100 nsec for the coefficients to converge, and the cost function J cannot fully converge to 0 and it stays around 0.1, but the eye is opened much wider than the distorted one.

We then applied our CMA equalizer to CD compensation, and the compensated eyes are shown in Fig. 13 for a 7-tap FFE. We investigated two fiber lengths of 75 km and 100 km with their distorted eyes given in Fig. 2. As a quantitative comparison, the CD distorted eye opening for 75-km fiber is from −0.75 to 0.4, while the CMA compensated eye opening is from −0.9 to 0.75, with 143% improvement. For 100-km fiber, the CD distorted eye opening is from −0.5 to 0.25, while the CMA compensated eye opening is from −0.9 to 0.6, with 200% improvement.

7 Conclusions

This paper presented rigorous channel models for various fiber dispersions and investigated their mitigations using digital and analog electronic equalizers. A novel CMA-based blind electronic equalization technique is proposed. While LMS feedback algorithm requires a training sequence to obtain the equalizer coefficients, the blind equalization automatically finds the optimal tap coefficients uti-

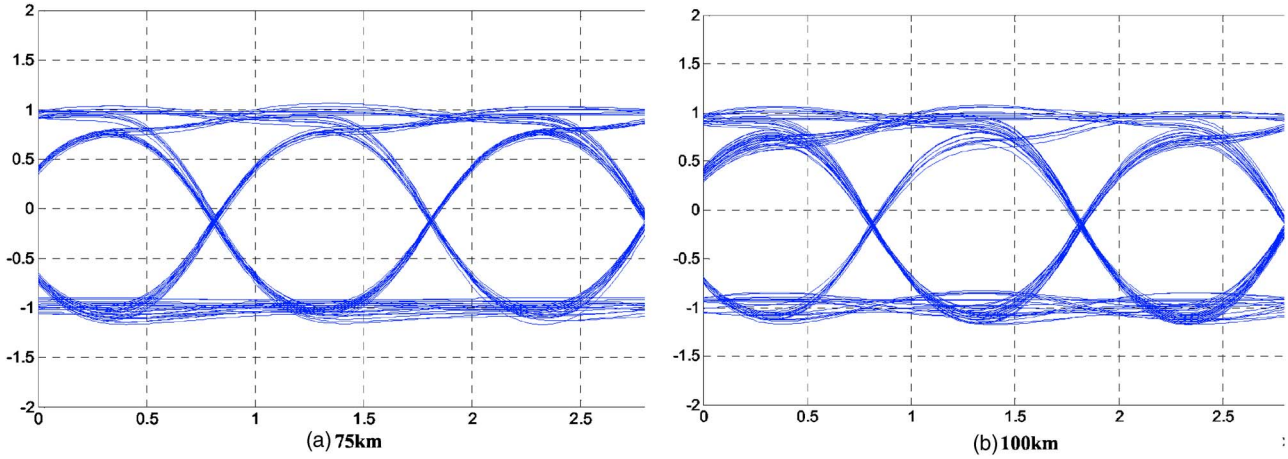

Fig. 13 CD compensation using a 7-tap FFE with blind CMA algorithm.

lizing the constant amplitude features in binary fiber transmissions. As a reference for LMS-based transversal equalizer design, the optimal tap coefficients for first-order PMD compensation have been summarized in Table 3. For CMA blind equalization, PMD compensation with DGD =80% symbol period and CD compensation with 200% eye-opening improvement were demonstrated. Also discussed is the adaptive fiber transceiver architecture with eye-open detectors that can be used to provide the feedback control for high-speed analog equalizers.

Acknowledgment

The author would like to thank Prof. J. K. Tugnait for valuable discussions on blind equalizations and S. F. Wei for assistance in simulations. Thanks are also due to the reviewers for their valuable suggestions and comments.

References

1. H. F. Haunstein, W. Sauer-Greff, A. Dittrich, K. Sticht, and R. Urbansky, "Principles for electronic equalization of polarization-mode dispersion," *J. Lightwave Technol.* **22**(4), 1169–1182 (2004).
2. K. Azadet, E. Haratsch, H. Kim, F. Saibi, J. Saunders, M. Shaffer, L. Song, and M. Yu, "Equalization and FEC techniques for optical transceivers," *IEEE J. Solid-State Circuits* **37**, 317–327 (2002).
3. H. Wu, J. Tierno, P. Pepeljugoski, J. Schaub, S. Gowda, J. Kash, and A. Hajimiri, "Integrated transversal equalizers in high-speed fiber-optic systems," *IEEE J. Solid-State Circuits* **38**, 2131–2137 (2003).
4. U. Koc and Y. Chen, "Adaptive opto-electronic compensator for excessive filtering, chromatic and polarization mode dispersion," *Opt. Fiber Commu. Conf.* **4**, 6–11 (2005).
5. M. Shirasaki, A. N. Akhter, and C. Lin, "Virtually imaged phased array with graded reflectivity," *IEEE Photonics Technol. Lett.* **11**(11), 1443–1445 (1999).
6. A. E. Willner, K.-M. Feng, S. Lee, J. Peng, and H. Sun, "Tunable compensation of channel degrading effects using nonlinearly chirped passive fiber Bragg gratings," *IEEE J. Sel. Top. Quantum Electron.* **5**(5), 1298–1311 (1999).
7. R. Khosravani et al., "Time and frequency domain characteristics of polarization-mode dispersion emulators," *IEEE Photonics Technol. Lett.* **13**(2), 127–129 (2001).
8. G. J. Foschini, L. E. Nelson, R. M. Jopson, and H. Kogelnik, "Probability densities of second-order polarization mode dispersion including polarization dependent chromatic fiber dispersion," *IEEE Photonics Technol. Lett.* **12**(3), 293–295 (2000).
9. G. J. Foschini, L. E. Nelson, R. M. Jopson, and H. Kogelnik, "Statistics of second-order PMD depolarization," *J. Lightwave Technol.* **19**(12), 1882–1886 (2001).
10. C. D. Poole and R. E. Wagner, "Phenomenological approach to polarization dispersion in long single-mode fibers," *Electron. Lett.* **22**, 1029 (1986).
11. B. L. Heffner, "Accurate, automated measurement of differential group delay dispersion and principal state variation using Jones Matrix Analysis," *IEEE Photonics Technol. Lett.* **5**, 814 (1993).
12. F. F. Dai and M. Pacek, "A hybrid integrated solution for chromatic and polarization mode dispersion compensation in high data rate fiber communications," *US Patent Application Publication*, No. 2003/0011847 A1, Jan. 16 (2003).
13. V. Kakani, F. F. Dai, and R. C. Jaeger, "A high speed integrated equalizer for dispersion compensation in 10 Gb/s fiber networks," *IEEE Intl. Symp. Circuits and Syst. (ISCAS)*, pp. 1178–1181, IEEE (2005).
14. F. F. Dai, S. Wei, and R. C. Jaeger, "Integrated blind electronic equalization for fiber dispersion compensation," *IEEE Intl. Symp. Circuits and Syst. (ISCAS)*, pp. 5750–5753, IEEE (2005).
15. J. R. Treichler and B. G. Agee, "A new approach to multipath correction of constant modulus signals," *IEEE Trans. Acoust., Speech, Signal Process.* **ASSP-31**, 459–472 (1983).
16. C. Richard Johnson Jr., P. Schniter, T. J. Endres, J. D. Behm, D. R. Brown, and R. A. Casas, "Blind equalization using the Constant Modulus Criterion: A review," *Proc. IEEE* **86**(10), 1927–1950 (1998).
17. H. Bulow, F. Buchali, and G. Thielecke, "Electronically enhanced optical PMD compensation," *Proc. Eur. Conf. Opt. Commu. (ECOC)*, pp. 39–40 (2000).
18. H. Bulow, "Electronic equalization of transmission impairments," *Opt. Fiber Comm. Conf. (OFC)*, pp. 24–25 (2002).
19. J. Sewter and A. Carusone, "A comparison of equalizers for compensating polarization-mode dispersion in 40-Gb/s optical systems," *IEEE Intl. Symp. Circuits and Syst. (ISCAS)*, pp. 1521–1524, IEEE (2005).

Foster F. Dai received his PhD degree in electrical engineering from The Pennsylvania State University, PA, in 1998. From 1986 to 1989, he was a lecturer at the University of Electronic Science and Technology, Chengdu, China. From 1989 to 1993, he was with the Technical University of Hamburg, Germany, working on microwave theory and RF designs. From 1997 to 2000, he was with Hughes Network Systems of Hughes Electronics, Germantown, Maryland, where he was a member of the technical staff in very large scale integration (VLSI), designing analog and digital ICs for wireless and satellite communications. From 2000 to 2001, he was with YAFO Networks, Hanover, Maryland, where he was a technical manager and a principal engineer in VLSI designs, leading high-speed SiGe IC designs for fiber communications. From 2001 to 2002, he was with Cognio Inc., Gaithersburg, Maryland, designing radio frequency (RF) ICs for integrated multi-band wireless transceivers. From 2002 to 2004, he was an RFIC consultant for Cognio Inc. In August 2002, he joined the faculty of Auburn University in Auburn, Alabama, where he is currently an associate professor in electrical and computer engineering. His research interests include VLSI circuits for digital, analog, and mixed-signal applications, RFIC designs for wireless and broadband communications, ultra-high frequency synthesis and analog and mixed signal built-in self-test (BIST). He is the co-author of *Integrated Circuit Design for High-Speed Frequency Synthesis* (Artech House Publishers, Feb, 2006). Dr. Dai has served as a Guest Editor for *IEEE Transactions on Industrial Electronics*. He currently serves on the Technical Program Committees of the *IEEE Symposium on VLSI Circuits*, the *IEEE Custon Integrated Circuits Conference (CICC)*, the *IEEE Bipolar/BiCMOS Circuits and Technology Meeting (BCTM)* and the *IEEE Topical Meeting on Silicon Monolithic Integrated Circuits in RF Systems (SiRF)*.